Cation composition effects on oxide conductivity in the $Zr_2Y_2O_7$–Y_3NbO_7 system

2009 J. Phys.: Condens. Matter 21 405403

(http://iopscience.iop.org/0953-8984/21/40/405403)

J. Phys.: Condens. Matter **21** (2009) 405403 (12pp) doi:10.1088/0953-8984/21/40/405403

Cation composition effects on oxide conductivity in the $Zr_2Y_2O_7$–Y_3NbO_7 system

Dario Marrocchelli[1], Paul A Madden[2], Stefan T Norberg[3,4] and Stephen Hull[3]

[1] School of Chemistry, University of Edinburgh, Edinburgh EH9 3JJ, UK
[2] Department of Materials, University of Oxford, Parks Road, Oxford OX1 3PH, UK
[3] The ISIS Facility, Rutherford Appleton Laboratory, Chilton, Didcot, Oxfordshire OX11 0QX, UK
[4] Department of Chemical and Biological Engineering, Chalmers University of Technology, SE-412 96 Gothenburg, Sweden

E-mail: D.Marrocchelli@sms.ed.ac.uk

Received 21 July 2009, in final form 19 August 2009
Published 8 September 2009
Online at stacks.iop.org/JPhysCM/21/405403

Abstract

Polarizable interaction potentials, parametrized using *ab initio* electronic structure calculations, have been used in molecular dynamics simulations to study the effect of cation composition on the ionic conductivity in the $Zr_2Y_2O_7$–Y_3NbO_7 system and to link the dynamical properties to the degree of lattice disorder. Across the composition range, this system retains a disordered fluorite crystal structure and the vacancy concentration is constant. The observed trends of decreasing conductivity and increasing disorder with increasing Nb^{5+} content were reproduced in simulations with the cations randomly assigned to positions on the cation sublattice. The trends were traced to the influences of the cation charges and relative sizes and their effect on vacancy ordering by carrying out additional calculations in which, for example, the charges of the cations were equalized. The simulations did not, however, reproduce all of the observed properties, particularly for Y_3NbO_7. Its conductivity was significantly overestimated and prominent diffuse scattering features observed in small area electron diffraction studies were not always reproduced. Consideration of these deficiencies led to a preliminary attempt to characterize the consequence of partially ordering the cations on their lattice, which significantly affects the propensity for vacancy ordering. The extent and consequences of cation ordering seem to be much less pronounced on the $Zr_2Y_2O_7$ side of the composition range.

M This article features online multimedia enhancements

(Some figures in this article are in colour only in the electronic version)

1. Introduction

Oxide ion conducting materials are the subject of intensive research activity due to their technological applications in solid oxide fuel cells (SOFCs), oxygen separation membranes and gas sensors. Cubic, fluorite-structured, binary compounds of stoichiometry AO_2 are of particular interest, especially when some of the host cations are replaced by species of a lower valence to produce anion-deficient phases like $A^{4+}_{1-x}B^{3+}_{x}O_{2-x/2}$. These compounds have charge compensating vacancies which allow the remaining anions to move more rapidly throughout the crystal and this leads to impressive values of the ionic conductivity ($\sigma > 0.1\ \Omega^{-1}\ cm^{-1}$, at $T = 1500$ K) as observed in M_2O_3-doped ZrO_2 (M = Sc or Y) and M_2O_3-doped CeO_2 (M = Y or Gd).

At the simplest level the ionic conductivity would be expected to increase with the number of vacancies, but this is not the case. In $Zr^{4+}_{1-x}Y^{3+}_{x}O_{2-x/2}$ the conductivity decreases

with increasing x for $x > 0.16$ and, furthermore, for a given x the value of the conductivity depends on the identity of the dopant cation [1]. For example, $Zr^{4+}_{1-x}Sc^{3+}_{x}O_{2-x/2}$ is a better conductor than $Zr^{4+}_{1-x}Y^{3+}_{x}O_{2-x/2}$ [2]. These effects are due to a reduced mobility associated with the ordering of the vacancies, which may be influenced by vacancy–vacancy, vacancy–cation and cation–cation interactions. Bogicevic and co-workers [3] examined these effects in stabilized zirconias by using first-principles, zero temperature electronic structure calculations. They found that vacancy ordering is most strongly governed by vacancy–vacancy interactions, followed by vacancy–dopant and, weakest of all, dopant–dopant interactions. The influence of the identity of the dopant could be understood in terms of a balance between competing electrostatic and elastic effects, which are associated with differences in the cation charges and radii. They showed that the best way to minimize vacancy–dopant association is to choose dopants where the strain term (i.e. the dopant ionic radius relative to that of the host cation) counteracts the electrostatic interaction, rather than simply matching the ionic radii. Some of these factors have also been identified in other studies [4–7].

We have carried out molecular dynamics (MD) simulation studies of a similar class of materials with realistic polarizable interaction potentials [8], in order to examine the influence of these effects at the experimentally relevant temperatures ($\geqslant$1000 K). The interaction potentials are capable of accurately reproducing experimental conductivities etc, and long-range effects of strain are incorporated by our use of considerably larger simulation cells (typically $4 \times 4 \times 4$ unit cells but up to $10 \times 10 \times 10$) than are accessible in direct first-principles calculations. In the present work we focus on the ternary system $Zr_{0.5-0.5x}Y_{0.5+0.25x}Nb_{0.25x}O_{1.75}$ which retains a disordered fluorite structure with a constant vacancy count as x is varied (one in 8 oxide ions is 'missing'), which allows us to selectively study the effect of varying dopant cation charge and ionic radius (Nb^{5+} is significantly smaller than Y^{3+} since $R_{cat} = 0.74$, 0.84, 1.019 Å for Nb^{5+}, Zr^{4+} and Y^{3+} respectively [9]). Although the number of vacancies is fixed across the whole series, the conductivity changes by almost two orders of magnitude from $x = 0$ to 1 at 1000 K [10]. Furthermore, it was observed that the intensity of diffuse scattering, related to the lattice disorder, *decreases* as the conductivity *increases* which presented the prospect of linking structural (crystallographic) studies to the effects on the conduction mechanism and the conductivity.

Consequently, we have examined [8, 11] this system with a combination of impedance spectroscopy, powder neutron diffraction—including the analysis of the total scattering using bond valence sum constrained reverse Monte Carlo modelling (RMC) [12–14]—and MD simulations. The RMC analysis indicated that real-space configurations based on a fluorite structure with the dopant cations randomly arranged within the cation sublattice, i.e. a disordered fluorite (d-fluorite) structure, gave an excellent representation of the diffraction data across the composition range. The MD simulations were initiated from such d-fluorite configurations. They *accurately* reproduced the average structure extracted from the diffraction data using RMC at the level of the partial radial distribution and bond angle distribution functions. Furthermore, the simulations reproduced the temperature dependence of the experimental conductivity for $Zr_2Y_2O_7$ (i.e. the $x = 0$ system) and the trend of decreasing conductivity with increasing Nb content across the series. A substantial part of the present paper will be concerned with a detailed analysis of these simulations and examination of the chemical factors which contribute to this trend. These analyses enable us to track the competition between Coulomb and strain effects on the vacancy ordering in the d-fluorite structure and to explain the consequences for the ionic mobility.

Other considerations suggest, however, that these simulations may miss an important contributor to the conductivity of these materials. Small area electron diffraction (SAED) studies have been carried out on these (and related) materials by several groups [15–17]. This technique gives single-crystal diffraction information. The SAED studies show sharp diffuse scattering features at particular positions in reciprocal space which are the result of a structural modulation which is not intrinsic to the d-fluorite structure [15–17]. The diffuse peaks are associated with a pattern of strain caused by vacancy ordering and, according to some authors [15], to partial ordering of the dopant cations. The ordering is of intermediate range, one analysis suggesting a correlation length of ~22 Å in Y_3NbO_7 [15]. The diffuse peaks suggest a structure with a local ordering tendency in which the anion vacancies are aligned in pairs along the ⟨111⟩ directions within the $x = 1$ (Y_3NbO_7) composition, in a manner related to the pyrochlore structure. As $x \to 0$ ($Zr_2Y_2O_7$) the diffuse scattering changes and, as interpreted by Irvine *et al* [16], is associated with vacancy alignment along ⟨110⟩ directions, which resembles the situation within the C-type structure of Y_2O_3. According to these authors, the decrease in conductivity as $x \to 1$ is caused by the effects of these different patterns of vacancy ordering on the anion mobility, though no clear explanation of this structure–property relationship has been provided to date. To anticipate the story below somewhat, not all of these peaks are seen in diffraction patterns calculated from our d-fluorite simulations, even if they are initiated with configurations in which the oxygen ions are placed in positions consistent with the pyrochlore vacancy ordering. We have, therefore, been led to perform a new set of simulations in which we explore the effect of some degree of local cation ordering.

In this paper, we begin with a detailed examination of the structure and ion dynamics in the d-fluorite simulations which successfully reproduce the trends observed in these properties in the $Zr_{0.5-0.5x}Y_{0.5+0.25x}Nb_{0.25x}O_{1.75}$ series. In order to clarify how they are affected by the cation properties, we consider the effects of modifying our *ab initio*-based interaction potentials by equalizing the cation charges and the range of the short-range repulsive interactions between the cations and the oxide ions. We then consider the structure of the material from the perspective of the vacancies and demonstrate similar cation-specific vacancy ordering tendencies to those which have been seen in the *ab initio* studies of stabilized zirconias [3]. For the reasons described above, we are then led to examine the consequences of partially ordering the cations for the energetics, the diffuse scattering and the conductivity. The

studies here are less definitive than the d-fluorite ones, as we cannot determine the degree of ordering within our MD simulations and must rely on drawing conclusions from different postulates for the order. The partially ordered structures necessarily have a lower entropy than the fully disordered ones, and therefore become unstable with respect to them at high temperatures. However it is only at very high temperatures (where these phases are unstable) that the cations move sufficiently to allow the structure to equilibrate.

2. Disorder and mobility in the d-fluorite structure of $Zr_2Y_2O_7$ and Y_3NbO_7

The simulation methodology is summarized in appendix A. The simulations are thoroughly equilibrated at high temperatures (1500–2000 K) in constant pressure simulations before obtaining dynamical information from constant volume runs at the zero-pressure volume. At these high temperatures the oxide ions are diffusing on the simulation timescale but there is no significant exchange of cations. We also quenched down to room temperature and conducted further short runs in order to examine structural information and compare with diffraction data collected at the same temperature. Note that, because the ionic mobility drops sharply as the temperature is reduced during the quench, that these runs are not fully equilibrated. To some extent, this will also be true of experimental samples which are prepared at high temperature and quenched, though the rate of cooling is much slower than for the simulated systems.

We begin by discussing results on the d-fluorite structure, which are initialized by randomly distributing the cation species over the cation sublattice and randomly assigning oxide anions to the anion lattice. Theoretical calculations show the energy scale associated with cation ordering is very small [3, 18] in yttria-stabilized zirconia and, as we showed in the previous paper [8], extensive powder diffraction and RMC analyses across the whole series $Zr_{0.5-0.5x}Y_{0.5+0.25x}Nb_{0.25x}O_{1.75}$ provided no evidence for cation ordering, in agreement with previous studies [10]. We also demonstrated the excellent agreement between the present simulations and the RMC data, as well as a very good reproduction of the temperature dependence of the experimental conductivity for $Zr_2Y_2O_7$. In the present paper we will only discuss results for the end members ($x = 0$ and 1) of the series, i.e. $Zr_2Y_2O_7$ and Y_3NbO_7.

2.1. Cation-induced disorder

The disordered character of the anion sublattice can be appreciated from the oxygen–oxygen radial distribution functions taken from the room temperature runs, $g_{O-O}(r)$ (see figure 1). They are compared with those expected from a perfect fluorite structure with the same lattice parameter (and with the $g_{O-O}(r)$ obtained from the RMC analysis of the experimental data [8]). The first peak in $g_{O-O}(r)$ for Y_3NbO_7 is shifted by 0.13 Å from the expected position for an ideal fluorite structure and the second peak (which indicates the distance between two next-nearest neighbouring oxygen ions)

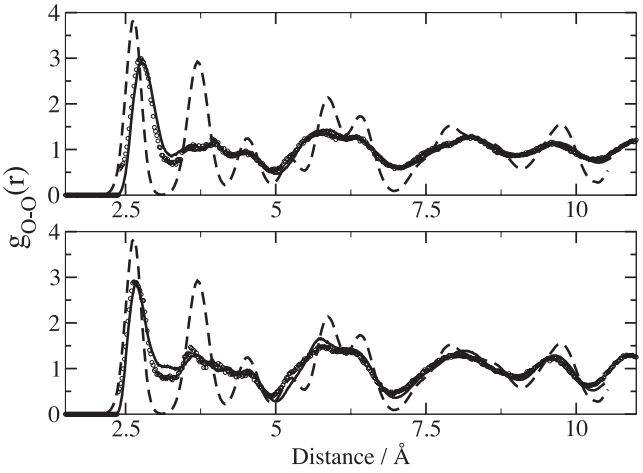

Figure 1. Comparison between the simulated (solid line) $g_{O-O}(r)$ (obtained from the QUAIM potential described in [8]) in $Zr_2Y_2O_7$ (bottom) and Y_3NbO_7 (top) and the one obtained from a perfect fluorite structure (dashed line) at room temperature. The experimental data (dots) from [8] obtained via bond valance sum constrained RMC are shown as well.

is broadened and presents a number of subsidiary features. $Zr_2Y_2O_7$ shows similar but less marked deviations from the ideal fluorite order, as already noted from the diffuse scattering intensity [8, 10].

In the fluorite structure, the anions sit in a tetrahedral site. Because the cation species are distributed randomly in the d-fluorite $Zr_2Y_2O_7$–Y_3NbO_7 system, the vertices of these tetrahedra may be occupied by different combinations of cations. A snapshot of the simulation cell in Y_3NbO_7 can be seen in figure 2. The two black circles highlight those oxide ions that are surrounded by Y^{3+} cations only and the red squares those with a significant number of Nb^{5+} ions in their coordination environment. Notice that the former are much more tightly grouped about the lattice site than the latter. The notion that the Nb^{5+} cations are somehow responsible for the disorder observed in Y_3NbO_7 is confirmed by the fact that the Y–O and Nb–O distances, obtained from the RMC analysis of the neutron scattering data in [8] (or analogously from our simulations), are quite different ($d_{Nb-O} = 1.96$ Å, $d_{Y-O} = 2.28$ Å). In a perfect fluorite structure, the anion–cation distance is $d_{an-cat} = \sqrt{3}/4\ a = 2.27$ Å, where a is the lattice parameter obtained from the RMC analysis. It is therefore evident that the Nb^{5+} ions are attracting the oxygen ions very tightly, thus disrupting the perfect fluorite order. This effect is less significant in $Zr_2Y_2O_7$ because the cation charges are 3+ and 4+ in this case and because the cation radii are more similar.

2.2. Cation effects on anion mobility

The inhomogeneities induced by this strain lead to a significant difference in conduction mechanisms between $Zr_2Y_2O_7$ and Y_3NbO_7. In figure 3 we show the probability distribution (calculated as in [8]) for the individual oxide ions to make a certain number of diffusive hops (by the O–O nearest-neighbour separation) during the course of the simulations

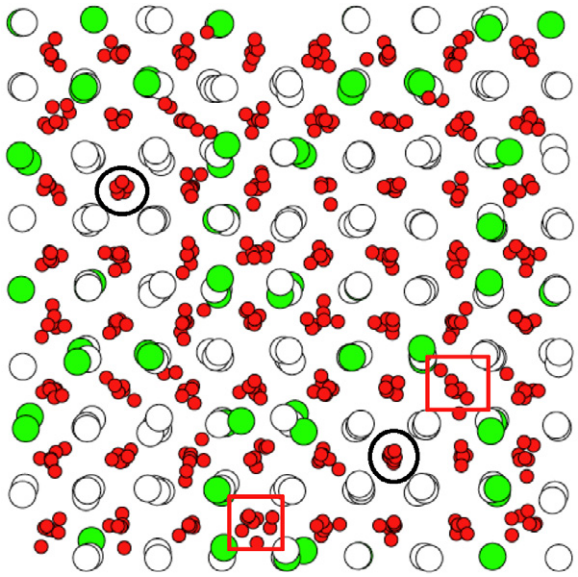

Figure 2. Snapshot along the z axis of the simulation box in Y_3NbO_7. The colour code is white, green and red for yttrium, niobium and oxygen ions respectively. (In black and white, the colour code is white, light grey and dark grey for yttrium, niobium and oxygen ions respectively.) The two black circles show those oxygen ions which are surrounded by yttrium ions only, whilst the two red squares show those which are surrounded by both niobium and yttrium ions.

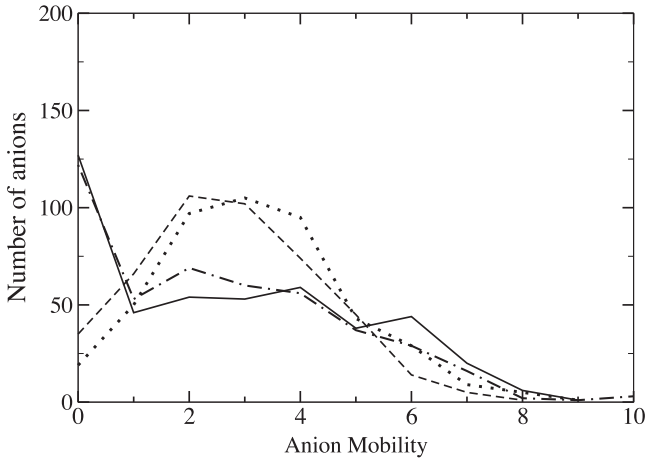

Figure 3. Number of ions with certain mobility against the mobility itself for Y_3NbO_7 (solid line), $Zr_2Y_2O_7$ (dashed line), equal-charge Y_3NbO_7 (dotted line) and equal-radius Y_3NbO_7 (dot–dashed line).

at 1500 K. In Y_3NbO_7 a large fraction of anions do not hop at all during the whole simulation whereas a few anions possess a high mobility. The former make no contribution to the conductivity. $Zr_2Y_2O_7$, on the other hand, has a more homogeneous behaviour with fewer immobile oxygen ions and a probability distribution which peaks about the average mobility of 2–3, with relatively few outliers. Further examination (see below) shows that the immobile oxide ions in Y_3NbO_7 are in tetrahedral sites where all the vertices are occupied by Y^{3+} cations.

As a consequence, the conductivity in Y_3NbO_7 exhibits an 'ageing' effect, especially at low temperatures. The average mobility shortly after initializing the simulation with randomly placed oxide ions is high, but drops over a substantial period of time ($\sim$1 ns) presumably because, on this timescale, oxide ions find initially empty Y^{3+}-rich sites and become trapped there. Another consequence is that different initial configurations give different mean diffusion coefficients even after very long runs. This is probably caused by the variation in the numbers of different types of tetrahedral sites in the initializations. Both of these effects make a reliable determination of the conductivity difficult for Y_3NbO_7 in the temperature range ($<$1500 K) where experimental measurements have been made. Our best efforts give a conductivity ($\sigma_{NE} = 0.016\ \Omega^{-1}\ cm^{-1}$ at 1500 K, where the subscript NE denotes Nernst–Einstein, see below) of about an order of magnitude larger than measured [8, 10]. This value is much lower than the one obtained for $Zr_2Y_2O_7$ ($\sigma_{NE} = 0.08\ \Omega^{-1}\ cm^{-1}$), which agrees with the experimental trend [8]. For $Zr_2Y_2O_7$ neither of these effects is observed and reliable conductivity values can be obtained down to the highest temperatures at which measurements are available[5]. In this case the slope of conductivity versus inverse temperature agrees very well with experiment and the actual value at 1500 K is only slightly larger than experiment (by a factor of less than 2 for the data in [10]).

The above-mentioned conductivity values were calculated from the ionic diffusion coefficients by using the Nernst–Einstein formula

$$\sigma_{NE} = \frac{c^2 \rho D}{k_B T} \tag{1}$$

where c is the charge, ρ the number density and D the diffusion coefficient of the mobile species, k_B is the Boltzmann constant and T is the temperature. The diffusion coefficients themselves have been calculated from the long time slopes of a plot of the mean-squared displacement (msd) of individual ions versus time. The Nernst–Einstein formula assumes that the ions move independently, which can only be approximately true in reality. A better value for the conductivity is obtained, in principle, from an integral over the charge current correlation function $J(t)$ [19]:

$$\sigma = \frac{1}{k_B T V} \int_0^\infty J(t)\, dt \tag{2}$$

though this quantity has very poor statistics, especially when diffusion is slow. We were able to get a reliable value of the true conductivity from very long runs ($>$1 ns) on the most highly conducting $Zr_2Y_2O_7$ system. At 1500 K $\sigma = 0.05\ \Omega^{-1}\ cm^{-1}$ which is 1.6 times smaller than the Nernst–Einstein value and in much better agreement with the experimental values in [8, 10]. At higher temperatures the differences between the two methods of calculating the conductivity become smaller.

[5] There is a lower limit to the values of the diffusion coefficient and conductivity which may be determined from the mean-squared displacement of the ions as a function of time. To be reliable, the ions must on average be diffusing by more than a lattice parameter, and when the mobility is very low this requires the mean-square displacement to be measured over a very long time and eventually longer than we can afford to simulate.

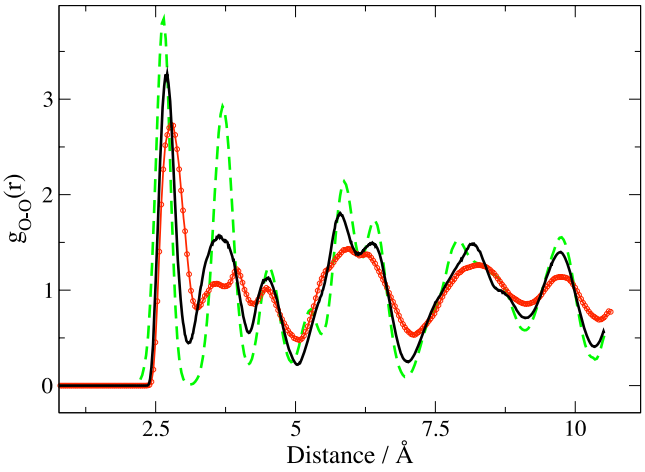

Figure 4. Comparison between the oxygen–oxygen $g(r)$ for Y_3NbO_7 (red dotted line), equal-charge Y_3NbO_7 (black solid line) and a perfect fluorite structure (red dashed line).

3. The effects of cation charges and sizes on the material's properties

The simulations on the $Zr_{0.5-0.5x}Y_{0.5+0.25x}Nb_{0.25x}O_{1.75}$ series in the d-fluorite structure give the same trend of decreasing conductivity and increasing disorder with increasing x that is seen experimentally. In this section we will attempt to distinguish the effects of cation size and charge by comparing the results obtained with modified interaction potentials with the realistic models.

3.1. The effect of the cation charge

In order to examine the role of the high charge of the Nb^{5+} cation in causing these effects we have carried out simulations on the $x = 1$ system in which both the 'Nb' and 'Y' ions are assigned a charge of 3.5+ (which maintains charge neutrality for this stoichiometry). We will call this system *equal-charge* Y_3NbO_7. All other aspects of the interaction potentials were kept the same (see appendix A) as in the runs described above. We started from a previous high temperature simulation on Y_3NbO_7 and equalized the cation charges. All the simulations were equilibrated at constant pressure for 100 000 steps, during which the velocities were rescaled several times to keep the system at the required (high) temperatures for conductivity studies, and then longer (constant volume) runs were made to study the properties of this material. We also ran some shorter simulations at room temperature to study the static structure and obtain the radial distribution functions.

In figure 4 we show the oxygen–oxygen radial distribution functions for room temperature *equal-charge* Y_3NbO_7, Y_3NbO_7 itself, and a perfect fluorite structure with a matched lattice constant. It is clear that equalizing the cation charges increases the order of the oxide ion sublattice[6]. The $g_{O-O}(r)$ for the equal-charge system shows a first peak close to the ideal fluorite position and a single prominent second peak, though still not as intense as in the ideal case. We also find that the cation–anion distances change significantly, $d_{Y-O} = 2.23$ Å and $d_{Nb-O} = 2.19$ Å. This is another sign that the system has become more ordered, as these become closer to the ideal cation–anion distance in this system, given, in this case, by $\sqrt{3}/4\ a_{equal-charge} = 2.27$ Å. A comparison between figure 4 and figure 1 shows that *equal-charge* Y_3NbO_7 is also more ordered than $Zr_2Y_2O_7$ which is consistent with the fact that $Zr_2Y_2O_7$ still has two cations with different charges (4+ and 3+).

[6] A movie (available at stacks.iop.org/JPhysCM/21/405403) can be found in the online version of this paper which shows how Y_3NbO_7 becomes more ordered once the cation charges are equalized.

Table 1. Diffusion coefficients.

Material	$10^6 \times D_O$ (cm^2 s^{-1})	
Y_3NbO_7	0.924	$T = 2000$ K
Equal-charge Y_3NbO_7	1.87	
$Zr_2Y_2O_7$	2.87	
Y_3NbO_7	0.072	$T = 1500$ K
Equal-charge Y_3NbO_7	0.21	
$Zr_2Y_2O_7$	0.44	
Equal-radius Y_3NbO_7	0.37	
Equal-charge and radius Y_3NbO_7	2.6	

Figure 3 shows that equalizing the cation charges (dotted line) greatly reduces the number of immobile oxide ions, relative to Y_3NbO_7. In fact, the distribution comes to resemble that for $Zr_2Y_2O_7$ quite closely and is indicative of a homogeneous pattern of diffusion. The mean-squared displacement for the oxide ions in *equal-charge* Y_3NbO_7 was calculated at 1500 and 2000 K and the respective diffusion coefficients are reported in table 1. From this it can be seen that *equal-charge* Y_3NbO_7 is more conducting than Y_3NbO_7. Interestingly *equal-charge* Y_3NbO_7 has a lower diffusion coefficient than $Zr_2Y_2O_7$, whereas we have just seen that the latter system has a more disordered oxide ion lattice. This suggests that there is some other factor at work besides the charge-induced strain in the lattice.

In order to see *how* the dopant cation charge induces the disorder and affects the ionic mobility we calculated the mobility distribution as done in [8] but this time we also monitored the identities of the four cations surrounding the anion. As already anticipated above, the anions with no mobility (about 1/4 of the total number, see figure 3) are in sites with a much higher Y^{3+} content than expected (≈3.65 as opposed to the average of three Y^{3+} and one Nb^{5+} which is expected from the Y_3NbO_7 stoichiometry) and the higher the mobility the higher the content of Nb^{5+} ions in the tetrahedron surrounding the anion. This effect seems to be associated with the *volume* of the coordination tetrahedron (obtained from the volume of the tetrahedron with the four closest cations at its vertices). The Coulombic repulsion between two Nb^{5+} ions is almost three times stronger than that between the Y^{3+} cations and from the cation–cation radial distribution functions we find that the nearest-neighbour cation–cation separations are $d_{Y-Y} = 3.69$ Å and $d_{Nb-Nb} = 3.86$ Å (the ideal fluorite value being $a/\sqrt{(2)} = 3.78$ Å) so that the coordination tetrahedra are strained to an extent which depends on their

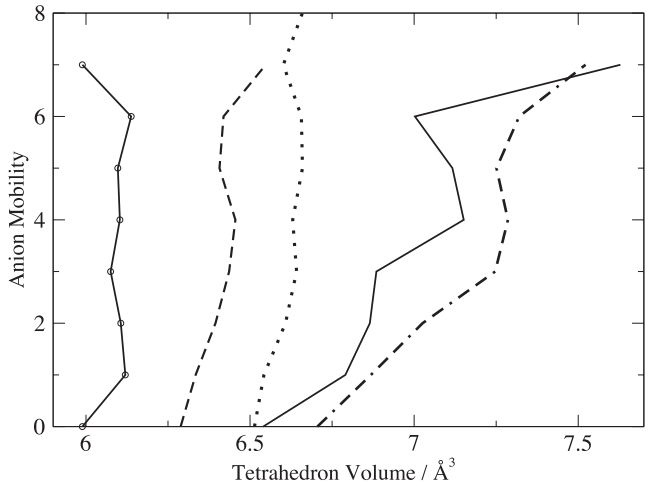

Figure 5. Anion mobility as a function of the average tetrahedron volume for *equal-charge* (dashed line), equal-radius (dot–dashed line), *equal-charge* and radius Y_3NbO_7 (circles + line), Y_3NbO_7 (solid line) and $Zr_2Y_2O_7$ (dots).

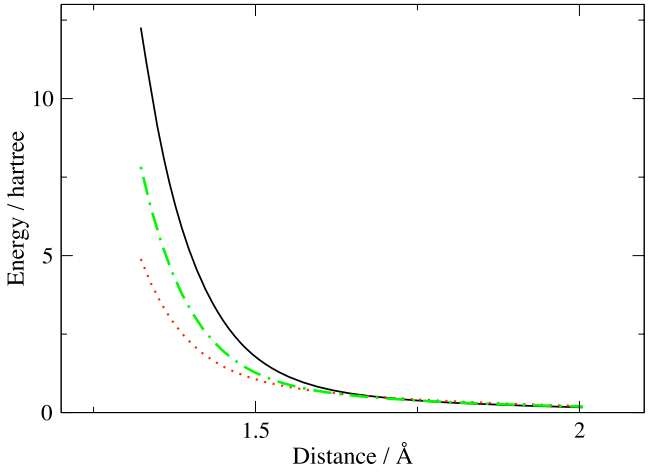

Figure 6. Short-range repulsion parts of the potential for the Y–O (solid line), Nb–O (dotted line) and Zr–O (dot–dashed line) terms.

Nb^{5+} content with the Nb^{5+}-rich ones significantly larger than the average. The anion mobility is plotted against the average volume of the surrounding tetrahedra in figure 5 (solid line). Alternatively, we could have plotted the mobility against the average number of Nb^{5+} ions in the coordination shell and obtained a very similar curve. Note, firstly, that the tetrahedral volumes for Y_3NbO_7 span an appreciable range, from 6.4 to 7.5 Å^3 and secondly, that the anion mobility is a strongly increasing function of the tetrahedron volume. This observation therefore explains the paradox that although highly charged Nb^{5+} cations bind oxide ions strongly they promote *local* mobility but reduce the overall conductivity by straining the cation sublattice resulting in the formation of oxide ion trapping sites. We also carried out the same analysis for $Zr_2Y_2O_7$ (dotted curve) and for *equal-charge* Y_3NbO_7 (dashed curve) and present the results in figure 5. In these cases, the range of tetrahedron volumes is much narrower than for Y_3NbO_7 (<0.2 Å^3) suggesting a much less strained cation lattice and the dependence of the anion mobility on the tetrahedral volume is barely discernible.

3.2. The effect of the cation size

Proceeding by analogy with the *equal-charge* study, we can examine the effect of equalizing the cation radii in Y_3NbO_7. The short-range repulsion terms in our potentials model the repulsion between two ions and therefore are intrinsically related to the extent of the valence electron density around the ion. In figure 6 we show the short-range repulsion terms for the Y–O, Nb–O and Zr–O interactions (recall that these were generated with the *ab initio* force-fitting strategy). It can be seen that the range of these potentials is consistent with the fact that Y^{3+} is the largest ion, Nb^{5+} the smallest, with Zr^{4+} of intermediate size. To generate an equal-radius model for Y_3NbO_7 we used the Zr–O short-range interaction parameters for the Y–O and Nb–O terms, but the Y^{3+} and Nb^{5+} ions keep their formal charges[7]. Simulations are run as previously described for the equal-charge case.

The partial radial distribution functions for *equal-radius* Y_3NbO_7 looks quite similar to the one obtained for Y_3NbO_7 itself (figure 1 and reference [8]) and we have not shown them separately. Despite the equal-radius potential construction, even the anion–cation distances are comparable (d_{Nb-O} = 1.93 Å, d_{Y-O} = 2.29 Å) to those of the parent compound. This confirms that the observed disorder is caused by the different cation charges in Y_3NbO_7 and that the different ranges of the repulsive cation–anion interactions do not play an important role. Given this similarity in structure, it is not surprising that the equal-radius system shows a wide range of tetrahedral volumes like Y_3NbO_7 itself and figure 5 (dot–dashed line) shows that, again, the oxide ion mobility tracks the tetrahedral volume like the parent compound. This leads to the inhomogeneous distribution of hopping probabilities, as shown in figure 3 (dot–dashed line) with a substantial fraction of immobile ions.

In table 1 we report the average diffusion coefficient obtained from a simulation at 1500 K on *equal-radius* Y_3NbO_7 and compare this value with *equal-charge* Y_3NbO_7, Y_3NbO_7 and $Zr_2Y_2O_7$ at the same temperature. Interestingly, the equal-radius material is more conducting than both *equal-charge* Y_3NbO_7 and Y_3NbO_7 though not as conducting as $Zr_2Y_2O_7$. That *equal-radius* Y_3NbO_7 is more conducting than Y_3NbO_7 itself is probably to be expected, what is more surprising is that it is also more conducting the *equal-charge* system which, as we have seen, has the kind of homogeneous distribution of mobilities seen in the highly conducting $Zr_2Y_2O_7$ system. This is probably a consequence of using the Zr–O short-range interaction parameters for the Y–O and Nb–O terms. As we mentioned above, these are

[7] Note that the Y–O and Nb–O nearest-neighbour separations which result from these simulations will differ, because of the stronger Coulombic attraction to the Nb^{5+} ion. From an empirical perspective, i.e. the way that the ionic radius is normally assigned, the ions do not appear as of equal size; rather they have been treated as if the electron density distributions around the ions are of equal size in the potential model.

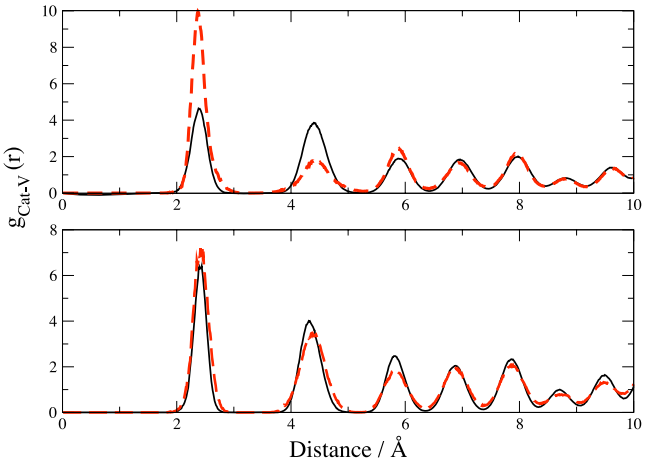

Figure 7. Yttrium–vacancy (solid line) and niobium–vacancy (dashed line) radial distribution functions in d-fluorite-structured Y_3NbO_7 (top) and equal-charge Y_3NbO_7 (bottom).

softer than the ones for the Y–O interaction but harder than the Nb–O ones. However, since in this system there are three times more Y^{3+} ions than Nb^{5+} ions, this means that, on average, the anion–cation short-range repulsion in this system is softer and this greatly enhances the anion mobility. A similar phenomenon was observed in the case of GeO_2 where rescaling the short-range interaction terms by a factor of 1.6 enhances the oxide ion diffusivity by several orders of magnitude [20].

As a final model system, we equalize both the cation radii and charges simultaneously (i.e. we use the Zr–O potential for all short-range interactions and set all cation charges equal to 3.5+). As might be expected this gives a small distribution of tetrahedral volume sizes (figure 5, line with circles) and virtually no oxide ion trapping. This material is an incredibly good ionic conductor with a conductivity of $\sigma_{NE} \approx 0.6\ \Omega^{-1}\ cm^{-1}$ at 1500 K, a value higher than the one found in the best yttria-stabilized zirconias ($\sigma \approx 0.6\ \Omega^{-1}\ cm^{-1}$ at 1667 K for 8% YSZ [21]).

4. Vacancy ordering effects

So far we have examined the relationship between disorder and mobility by examining the ionic positions and the effect of making particular changes in the interaction potential. In section 1, we motivated our study of this system by reference to the properties of the *vacancies* and the way they are ordered by their interactions with the ions. Their effect is, of course, implicit in the properties we have examined so far, but now we turn to an examination of the simulation trajectories by considering the vacancies explicitly.

4.1. Vacancy interactions

In appendix B we explain how we identify the vacancies and how we can obtain the ion–vacancy and vacancy–vacancy radial distribution functions. Integration of these can be used to define coordination numbers. For example, integrating the Y^{3+}–vacancy rdf, $g_{Y-V}(r)$, from zero out to the position, r_c, of first minimum of the $g_{Y-O}(r)$ gives the average number of vacancies in the first coordination shell of a Y^{3+} ion. In figure 7 we show the cation–vacancy radial distribution functions for Y_3NbO_7 and *equal-charge* Y_3NbO_7 at 1500 K. From this figure the tendency of the vacancies to bind to Nb^{5+} ions is clear for Y_3NbO_7. This tendency is strongly reduced when the cation charges are equalized.

Table 2. Cation–vacancy relative coordination numbers extracted from our MD simulations at 1500 K.

Material	n_{Y-V}	n_{Nb-V}	n_{Zr-V}
Random	1	1	1
Y_3NbO_7	0.81	1.53	
$Zr_2Y_2O_7$	0.79		1.21
Equal-charge Y_3NbO_7	0.92	1.23	
Partially ordered Y_3NbO_7	0.72	1.85	
Pyrochlore $Zr_2Y_2O_7$	0.15		1.85

In table 2 we report the number of vacancies around the different cations compared to the number which would be expected if the vacancies occupied sites randomly. It is clear from the table that vacancies bind very strongly to Nb^{5+} ions in d-fluorite Y_3NbO_7 and less strongly to Zr^{4+} in $Zr_2Y_2O_7$. Considering the Coulombic effects, the vacancies (which have a relative charge of 2+) would be expected to bind more strongly to the cation with the lowest charge, i.e. Y^{3+} in both materials. The fact that the contrary happens is therefore indicative of the importance of strain effects which are strong enough to outweigh the Coulombic interactions [3], i.e. the vacancies prefer to bind to the smallest cations, despite their higher charges. This is confirmed by solid-state NMR studies [22] on yttria-doped zirconias.

We may now extend this analysis to examine the vacancy–vacancy ordering by integrating g_{V-V} between limits which bound the different coordination shells around an anion site in an ideal fluorite lattice. The first such shell gives the probability of finding a pair of vacancies as nearest-neighbours (i.e. along the ⟨100⟩ direction of the fluorite lattice) whereas the second shell relates to vacancy pairs along ⟨110⟩ and the third to ⟨111⟩. These probabilities may be compared with what would be expected if the vacancies are randomly distributed on the simple cubic anion lattice and we give the ratios in table 3 for simulations at 1500 K. As we note in the appendix B, it is likely that the way that we identify vacancies leads to an overestimate of the number of vacancy nearest-neighbours. Nevertheless, it can be seen that there is a specific ordering tendency, with ⟨111⟩ vacancy pairs appearing with a higher frequency than would be expected for a random distribution, and nearest-neighbour pairs being lower. This order is in accord with Bogicevic's [3] examination of the energetics of vacancy ordering in lightly doped yttria-stabilized zirconia. The tendency we observe is, however, not as strong as might be expected from the calculations in this paper. This is, in part, due to the above-mentioned overestimate of the number of nearest-neighbours for algorithmic reasons, but is also because our calculations have been performed at high temperatures where the ordering is opposed by entropic effects. It is also interesting to notice that the vacancy ordering tendency decreases as temperature is raised and completely disappears at

Table 3. Relative population of the anion vacancy pairs expected from a random distribution of vacancies within a cubic fluorite lattice, compared with those extracted from our MD simulations at 1500 K.

Material	⟨100⟩	⟨110⟩	⟨111⟩
Random	0.231	0.461	0.308
Y_3NbO_7	0.191	0.418	0.390
$Zr_2Y_2O_7$	0.166	0.391	0.442
Equal-charge Y_3NbO_7	0.136	0.480	0.384
Partially ordered Y_3NbO_7	0.154	0.304	0.542
Pyrochlore $Zr_2Y_2O_7$	0.073	0.147	0.780

2000 K. Finally, this tendency seems to be stronger in $Zr_2Y_2O_7$ than in Y_3NbO_7 which might seem at first counterintuitive considering that $Zr_2Y_2O_7$ is a better conductor than Y_3NbO_7. This apparent contradiction will be explained in the next section.

4.2. *Effects of vacancy interactions on the diffuse scattering*

The vacancy ordering influences the diffuse scattering observed in diffraction studies, and it is useful to compare the consequences of the degree of vacancy ordering we find in the simulations with those seen experimentally. Our simulations have reproduced extremely well the structures derived from the analysis of the total (i.e. Bragg plus diffuse) *powder* diffraction [8] in these systems. However, several SAED studies [15, 16] have shown intense diffuse peaks for Y_3NbO_7 at particular positions in reciprocal space. This suggests that the vacancy ordering effects are considerably stronger and of longer range than is indicated by the propensities we have shown in tables 2 and 3. In order to compare with these experimental studies we have calculated the diffuse scattering from the ionic configurations available from the simulations as described in appendix C.

We decided to calculate the electron diffraction pattern of Y_3NbO_7 and $Zr_2Y_2O_7$ along the $[\bar{1}\bar{1}0]_f$ zone axis (f refers to the cubic fluorite structure). This is found to be the most informative pattern in the experimental studies [15–17]. In the experimental patterns of Y_3NbO_7, a pair of intense and closely spaced diffuse peaks is seen at $\mathbf{G_F} \pm \frac{1}{2}(111)^*$, where $\mathbf{G_F}$ is a reciprocal lattice vector of the fluorite-type lattice. In fact, the two peaks correspond to a ring of diffuse scattering centred at these positions which is projected down into the $[\bar{1}\bar{1}0]_f$ plane. The $\mathbf{G_F} \pm \frac{1}{2}(111)^*$ positions correspond to the location of Bragg peaks in the pyrochlore structure and the diffuse scattering seen in Y_3NbO_7 indicates a pattern of vacancy pairs along the $[111]_f$ direction which form strings along $[110]_f$, as in the pyrochlore structure, but of finite range[8]. In $Zr_2Y_2O_7$ the diffuse scattering is considerably weaker and the pattern of peaks is somewhat different. It appears as streaks along $[001]_f$ in the studies by Irvine *et al* [16] and taken as indicative of C-phase ordering of vacancies (i.e. vacancy pairs along $[110]_f$). Whittle *et al* [17], however, observe the pattern as three peaks centred at $\mathbf{G_F} \pm \frac{1}{2}(111)^*$ and interpret it as another type of pyrochlore-like modulated structure.

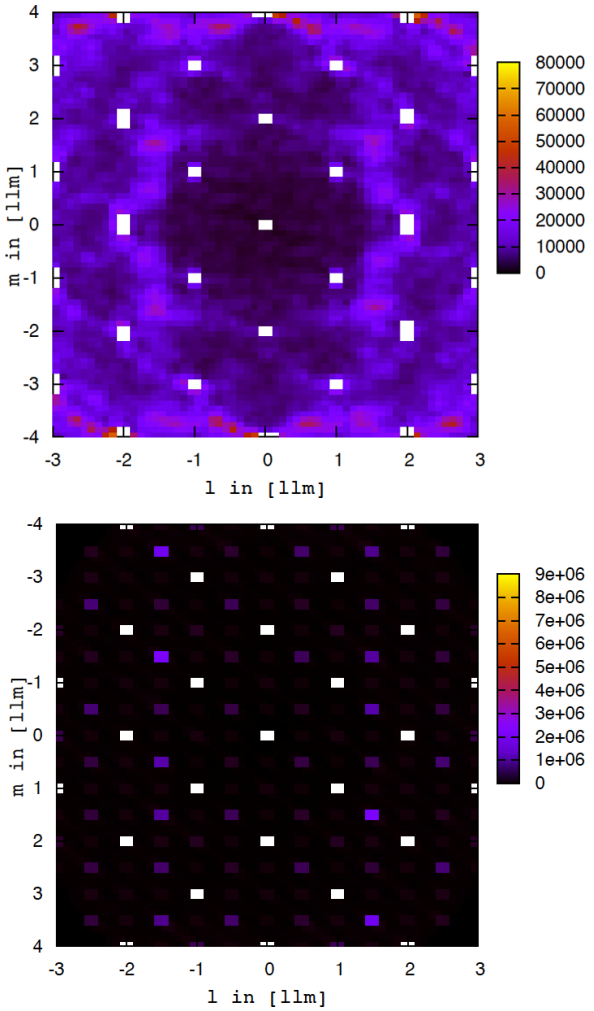

Figure 8. Electron diffraction pattern obtained from the MD data for d-fluorite (top) and locally cation-ordered (bottom) Y_3NbO_7.

In figure 8 we show the electron diffraction patterns calculated from our MD data (obtained from a simulation on 11 000 atoms, i.e. 10 × 10 × 10 unit cells). The pattern does not show the diffuse spots at $\mathbf{G_F} \pm \frac{1}{2}(111)^*$ which have been observed in the experimental SAED patterns [15–17]. The calculated patterns show some diffuse signal at some of these positions but this appears weaker and less sharply peaked than in the experimental studies. This finding was confirmed in longer MD simulations on smaller cells. As a test, we made a similar comparison with the diffuse neutron scattering [23] derived from single-crystal studies of $(ZrO_2)_{1-x}$–$(Y_2O_3)_x$ for $0.1 < x < 0.25$ and this was very successful, thus indicating that the disagreement with the experimental data is probably not a limitation of the way the diffuse scattering has been calculated.

[8] An ideal pyrochlore structure type, $A_2B_2O_7$, is a superstructure of the fluorite (MX_2) structure and is based upon a 2 × 2 × 2 unit cell with $Fd\bar{3}m$ symmetry (figures showing the differences between a fluorite and a pyrochlore structure can be found in [1, 17].) The cation superstructure of pyrochlore is based upon ordering of A and B cations parallel to the ⟨110⟩ directions, separated by $\frac{1}{2}\frac{1}{2}\frac{1}{2}$, with respect to the origin. The A and B cations are, respectively, found at the 16c (eight-coordinated) and 16d (six-coordinated) sites whereas the anions are distributed between two tetrahedrally coordinated positions: 48f [O(1)] and 8a [O(2)]. There is another tetrahedral site potentially available for the anions, 8b, which is systematically vacant in fully ordered pyrochlores.

For Y_3NbO_7 we prepared a starting configuration for an MD run in which the cations were distributed randomly over the cation sublattice but in which the oxide ions were placed as if in a pyrochlore structure, to give the associated vacancy-ordered structure. In simulations at 1500 K, this initial configuration rapidly evolved to one in which the extent of vacancy ordering had relaxed to that seen in the previous d-fluorite simulations. It therefore does not appear that we can reproduce the evidence for vacancy ordering from the SAED studies with simulations based upon the d-fluorite structure with randomly disposed cations.

In summary then, the d-fluorite simulations reproduce the experimentally observed *trends* in disorder and conductivity and have enabled us to account for the way that these properties are affected by the cation size and charge. However, there is a suggestion that these simulations overestimate the conductivities, especially on the Nb-rich side of the composition range. Furthermore, although the simulations demonstrate vacancy ordering tendencies similar to those which have been found in more lightly doped zirconias these are not sufficiently strong to reproduce the SAED patterns. We are therefore led to reconsider one of the underlying assumptions of the work described so far, namely that the different cation species are randomly distributed throughout the lattice.

5. Local cation ordering effects

Our simulation studies of Y_3NbO_7 in the d-fluorite structure have shown lattice distortions induced by the Nb^{5+} ions, especially when two or more Nb^{5+} ions are found as cation nearest-neighbours (the nearest-neighbour Nb^{5+}–Nb^{5+} distance is 3.86 Å as opposed to the ideal cation–cation distance in a fluorite structure $a/\sqrt{(2)} = 3.78$ Å). The strength of this effect would suggest that the system will try to adapt by ordering the Nb^{5+} ions so as to minimize the strain. Furthermore, the O–Nb–O bond angle distributions extracted from the MD and RMC-generated configurations suggested a tendency towards octahedral local anion coordination of the Nb^{5+} sites [8]. Motivated by these considerations and by our inability to reproduce the SAED patterns in Y_3NbO_7 we have been led to examine the consequences of *local* cation ordering in this system. Note that local (rather than long-ranged) ordering presents a significant problem for simulation studies because they necessarily involve periodic replication of a simulation cell which may be too small to allow for the decay of the structural correlations. Nevertheless, Miida *et al* [15] estimate the correlation length of the order responsible for the diffuse rings in the SAED pattern to be ∼22 Å which is the range of four fluorite unit cells (the majority of our d-fluorite simulations involved four unit cells along each Cartesian direction, though the 11 000 atom MD cells used in the initial comparison with SAED involved 10). Furthermore, in the calculations to be described below, the cation ordering is imposed upon the system, using intuition and also the insight from the SAED studies to guess a structure which will minimize the lattice strain. In future work we will attempt to use a Monte Carlo cation-swapping algorithm to set up the system in a less biased way [24].

The natural stoichiometry for a pyrochlore-structured oxide is $A_2B_2O_7$ where B is a smaller cation which prefers octahedral coordination and A a larger one which prefers 8 oxide neighbours. We have seen above that there is a tendency for the smaller Nb^{5+} and Zr^{4+} ions to preferentially bind vacancies and hence reduce their coordination number relative to Y^{3+}, and adoption of the pyrochlore arrangement would allow this tendency to be accommodated. Opposing this tendency may be long-range strain effects, such as that noted above involving Nb^{5+} in particular, and entropy, since the adoption of the pyrochlore structure involves ordering both the cation and anion sublattices with respect to d-fluorite. Jiang *et al* [18] estimate the configurational entropy as

$$\Delta S_{\text{ideal}} = -4k_{\text{B}}[x \ln x + (1-x)\ln(1-x) + 2y \ln y + 2(1-y)\ln(1-y)] \quad (3)$$

where x is stoichiometric ratio of cations ($\frac{1}{2}$ for $Zr_2Y_2O_7$ and $\frac{1}{4}$ for Y_3NbO_7) and y the fraction of vacancies to oxide ions in the unit cell $\frac{1}{8}$. This gives configurational entropies of 4.986×10^{-4} eV K^{-1} and 4.534×10^{-4} eV K^{-1} for $Zr_2Y_2O_7$ and Y_3NbO_7, respectively. $Zr_2Y_2O_7$ has the appropriate stoichiometry to adopt the pyrochlore structure but the radius ratio of the cations is not sufficiently large to allow a stable, long-range ordered structure to form [18]—certainly not at the temperatures at which the solid-state synthesis is carried out. The situation must be very marginal however, as $Hf_2Y_2O_7$ does form a pyrochlore [17, 18], and the Hf^{4+} ion is only slightly smaller than Zr^{4+} (note that Jiang *et al* [18] suggest that 'covalent' effects may play a role alongside ion size in this comparison). Some *local* pyrochlore-like ordering in $Zr_2Y_2O_7$ does therefore, seem plausible. The stoichiometry of Y_3NbO_7 is not that of a pyrochlore, but that does not rule out a pattern of local cation and vacancy ordering which is pyrochlore-like. Note that Irvine *et al* [16] consider *cation*-ordering in Y_3NbO_7 likely and Miida [15] has interpreted the SAED patterns by proposing modulated structures in which there is some local ordering of both vacancies and cations. The RMC-interpreted powder neutron studies [8] showed no evidence for cation ordering in either $Zr_2Y_2O_7$ or Y_3NbO_7, but it must be noted that the neutron scattering lengths of Y^{3+}, Zr^{4+}, and Nb^{5+} are very similar and therefore no evidence of cation ordering can be obtained with this technique.

5.1. Partially ordered Y_3NbO_7

As mentioned above, Y_3NbO_7 does not have the correct stoichiometry to adopt a pyrochlore structure. However, it seems reasonable to assume that the smaller Nb^{5+} ions will prefer to occupy the octahedrally coordinated B sites and we arranged the cations so that all the Nb^{5+} ions randomly occupy half of the B sites with the Y^{3+} occupying the remaining B sites as well as all the A sites. As a consequence of the random assignment of cations to the B sites the system does not exhibit 'long'-range cation order within the simulation cell (though, because of the simulation boundary conditions, the system is periodic). The oxide ions were placed in the O[1] and O[2] positions.

We ran a simulation on this material in the same way as explained above on a system with 11 000 atoms. The obtained electron diffraction spectrum is shown in figure 8. It can be appreciated that this pattern shows peaks at $\mathbf{G_F} \pm \frac{1}{2}(111)^*$, in reasonable agreement with the experimental data. The reason why we do not observe two diffuse spots but a single peak is that, because of the periodic boundary conditions, in reality we do have some long-range order in the cation positions.

We computed the internal energies of the partially cation-ordered Y_3NbO_7 d-fluorite at low temperatures ($T = 100$ K). This was done by slowly cooling a well-equilibrated high temperature run. These runs contained 704 atoms (four fluorite unit cells in each direction). We find that the locally ordered material has an energy which is lower by about $\Delta E \approx 56\ \mathrm{kJ\ mol^{-1}} = 0.58\ \mathrm{eV/molecule}$ than the d-fluorite material[9], confirming that some degree of cation ordering is indeed favoured on energetic grounds. From this we can calculate the order–disorder transition temperature, as in [18], $T_{\mathrm{O-D}} \approx \Delta E/\Delta S_{\mathrm{ideal}} = 1160$ K. This value goes up to $T_{\mathrm{O-D}} \approx 1460$ K if we assume that only 2/3 of the vacancies are ordered, i.e. if we set $y = 1/12$ in equation (3). Considering that this material is usually synthesized at 1700–1800 K [8, 15, 16], it seems plausible that a certain degree of cation ordering is observed depending upon how the sample is cooled back to ambient conditions.

We find that the locally ordered material is a much poorer ionic conductor than the disordered Y_3NbO_7. We estimate[10] that cation-ordered Y_3NbO_7 has a conductivity of $\sigma_{\mathrm{NE}} \leqslant 0.002\ \Omega^{-1}\ \mathrm{cm}^{-1}$ at 1500 K, approximately an order of magnitude lower than the d-fluorite simulations at the same temperature and in much better agreement with the experimental data. The reason for this much lower value of the conductivity is that a partial cation ordering increases the Nb^{5+}–vacancy association (see table 2) as well as the vacancy–vacancy pairing along the ⟨111⟩ direction (see table 3) and both factors hinder the vacancy mobility and therefore reduce the overall conductivity.

5.2. *Cation ordering in $Zr_2Y_2O_7$*

Cation ordering in $Zr_2Y_2O_7$, on the other hand, seems to be a less important issue. We recall that the tendency for Zr^{4+} to preferentially bind vacancies, relative to Y^{3+}, is considerably lower than for Nb^{5+} in Y_3NbO_7, and the strain associated with the different local cation configurations is much less pronounced in this system. The experimental SAED studies show slightly different diffuse scattering patterns [16, 17], suggesting that lattice modulations in this material depend on the details of sample preparation. In all cases, the diffuse features are less intense than in Y_3NbO_7. Whittle *et al* [17] have estimated a correlation length of ≈11 Å for the local order which is much smaller than in Y_3NbO_7.

Since $Zr_2Y_2O_7$ has the correct stoichiometry for a pyrochlore, we have run simulations starting from a fully pyrochlore-ordered configuration (i.e. a long-ranged ordered structure). The internal energy of this system at 100 K is slightly lower ($\Delta E = 49.5\ \mathrm{kJ\ mol^{-1}}$, a value in reasonable agreement with the trends observed in [18]) than that of a d-fluorite configuration obtained by cooling down a high temperature run and, considering that the ordered system has a lower entropy, it would seem that this structure is unlikely to become stable at higher temperatures (the estimated $T_{\mathrm{O-D}}$ is ≈1030 K). We also simulated the ordered system at 1500 K to calculate the conductivity (note that there is no cation site exchange at this temperature, so that the system cannot relax to d-fluorite on the simulation timescale). We find the conductivity to be very small (at least two orders of magnitude lower than the experimental value). An analysis of the vacancy–vacancy and cation–vacancy rdfs confirms that in pyrochlore-structured $Zr_2Y_2O_7$ there is a strong pairing of the vacancies along the ⟨111⟩ direction and that these bind very strongly to the Zr^{4+} cations (see tables 2 and 3) which explains the very small ionic conductivity shown by this sample.

6. Summary and conclusions

We initially examined d-fluorite simulations, with a disordered cation sublattice, which had been shown to reproduce very closely the neutron powder diffraction data [8], and these already allow us to account for a substantial part of the experimentally observed trends in the conductivity and degree of disorder between Y_3NbO_7 and $Zr_2Y_2O_7$. The difference between the two systems can be attributed to differences in cation size and to the different degree of strain imposed on the lattice by the highly charged cations—this creates oxide trapping sites in Y_3NbO_7 and gives an inhomogeneous character to the diffusive dynamics. Although both systems exhibit a tendency to order vacancies so that there is a likelihood of finding the vacancies close to the smaller cation, the vacancy ordering effects are not sufficiently strong to give rise to the diffuse scattering features which have been observed in small area electron diffraction studies. The fact that the observed trends are recovered from these d-fluorite simulations implies that they are primarily associated with the mean cation composition and traceable to the direct influence of ion size and charge, with any influence of intermediate-range vacancy structuring an additional feature.

Because the d-fluorite simulations failed to reproduce the diffuse scattering seen in SAED studies we were led to consider the possible effects of partial cation ordering based upon the pattern suggested by the pyrochlore crystal structure. Our results in this context are only indicative as we have, as yet, only examined the properties of 'by-hand' ordered systems. Nevertheless, in Y_3NbO_7 we were able to postulate a structure for which the diffuse scattering was in qualitative accord with the SAED diffuse scattering patterns and which was energetically favoured with respect to d-fluorite. In this structure the tendency of vacancies to bind to the smaller cation was considerably enhanced relative to d-fluorite and the conductivity was reduced by an order of magnitude, bringing it much closer to the experimental value. For $Zr_2Y_2O_7$ we were not able to postulate a partially ordered structure which

[9] This value is found to depend weakly on the cooling rate and on the system history.

[10] The error associated with this number is large because the corresponding mean-squared displacement curve is very noisy due to the low mobility of the anions.

would significantly improve upon the d-fluorite calculations across the full range of observations (including the SAED). In $Zr_2Y_2O_7$ the calculated conductivity in the d-fluorite structure is already close to the experimental value and the agreement with the powder diffraction data is very good. The SAED studies indicate that any intermediate-range order is weaker in this case and our own studies on d-fluorite show that the tendency for vacancies to associate with the smaller cation (the driving force for pyrochlore-like ordering) is considerably reduced relative to Y_3NbO_7. In this case a *fully* ordered pyrochlore is slightly favoured energetically over the d-fluorite structure but the entropy cost is high enough that the latter, more disordered structure, will be more stable above ≈1000 K.

As we have indicated above, the finding that partial cation ordering has an influence on the material properties presents a challenge for MD simulation because at the temperatures at which we might hope to equilibrate the system with respect to cation positioning the ordering tendency has disappeared for entropic reasons. However, the cation ordering also presents a challenge for comparing experimental results. The materials are synthesized at high temperatures but then cooled (according to different protocols) in different studies: as the temperature is reduced the cation mobility will be drastically reduced so that the degree of cation ordering found in low temperature studies will depart from the thermodynamic equilibrium value to varying extents.

Acknowledgments

We thank the EaStCHEM resource computing facility (http://www.eastchem.ac.uk/rcf) for computing resources and the Moray Endowment Fund of the University of Edinburgh for the purchase of a workstation. DM thanks the EPSRC, School of Chemistry, University of Edinburgh, and the STFC CMPC for his PhD funding. STN wishes to thank the EU Research and Technology Development Framework Programme for financial support.

Appendix A. Simulation details

We used dipole polarizable interaction potentials specified in [8] (known as DIPPIM). These interaction models include full, formal charges on the ions and the Nb^{5+}, Zr^{4+}, Y^{3+}, O^{2-} ions have their full, in-crystal polarizabilities. The parameters for these potentials were obtained by 'force-matching' them to *ab initio* reference data as described in [25]. The full set of parameters is reported elsewhere [8]. Most of the simulations on $Zr_{0.5-0.5x}Y_{0.5+0.25x}Nb_{0.25x}O_{1.75}$ were done using a cubic simulation box with 256 cations and 448 oxygen ions ($4\times4\times4$ unit cells) though some calculations were done with larger cells. The time step used was (unless otherwise specified) 20 au $= 4.84\times10^{-4}$ ps and all the runs were performed either in an NPT or NVT ensemble, with thermostats and barostats as described in [26]. Most of the high temperature runs were performed in an NVT ensemble, in which the cell volume was obtained from a previous run in an NPT ensemble with the external pressure set to zero. Coulombic and dispersion interactions were summed using Ewald summations while the short-range part of the potential was truncated to half the length of the simulation box, i.e. about 10 Å. All the simulations were between 110 ps and 10 ns long. We used an MPI version of our code which we mainly ran on a small workstation with two E5462 Xeon processors. One such processor would yield about 500 000 steps (i.e. ≈250 ps) in a day.

Appendix B. Vacancy identification and calculation of the vacancy–cation coordination numbers

We can identify the positions of vacancies for an instantaneous ionic configuration by finding which of the coordination tetrahedra are empty. Because the cations are not diffusing we can monitor the properties of each tetrahedron from the identities and instantaneous positions of the four cations which sit at its vertices. Such a tetrahedron is empty if no anion is within the volume bounded by the four planes defined by the positions of each set of three of the cations. Because the oxide ions may perform large amplitude vibrations about their average sites at the temperatures of interest for dynamical studies we only assign a vacancy to a tetrahedral site if the tetrahedron has been empty for a minimum of two frames (i.e. 10 fs). This measure has already been used for the study of PbF_2 [27, 28] and seems to identify vacancies reasonably faithfully even at high temperatures. For example, in simulations of $Zr_2Y_2O_7$ at 1500 K we find that the average number of vacancies is 86 whereas the stoichiometry would indicate 64. This number goes down to 67 at 300 K, in reasonable agreement with the stoichiometric value. Thermally excited Frenkel pairs may make a small contribution to the excess observed at high temperature but the most important factor is probably a shortcoming of our way of assigning vacancies. If a tetrahedral site contains a vacancy, it will induce a substantial distortion of surrounding tetrahedra which lowers the reliability of the geometric criterion we use to decide if the site is filled or empty, especially at high temperatures where all the atoms are making large amplitude vibrations. There is therefore a tendency to assign vacancies to sites which neighbour a site containing a true vacancy, and this is manifested in a larger than expected amplitude for the nearest-neighbour peak in the vacancy–vacancy radial distribution function discussed below.

Once vacancy positions have been identified we can calculate radial distribution functions (rdfs) between ions and vacancies and also vacancy–vacancy radial distribution functions. These are averaged over the entire run. Integration of the rdf can be used to define coordination numbers. For example integrating the Y^{3+}–vacancy rdf, g_{Y-V} from zero out to the position r_c of first minimum of the g_{Y-O} rdf gives the average number of vacancies in the first coordination shell of a Y^{3+} ion, n_{Y-V}

$$n_{Y-V} = 4\pi\rho\int_0^{r_c} \mathrm{d}r\, r^2 g_{Y-V}(r), \tag{B.1}$$

where ρ is the density of vacancies. Analogously, integrating the vacancy–vacancy rdf, g_{V-V} from zero out to the position r_c of first minimum of the g_{V-V} rdf gives the average number of vacancies in the first coordination shell of another vacancy.

Appendix C. Diffuse scattering calculation

We calculate the intensity of (total) scattering at a point **q** in reciprocal space from

$$I(\mathbf{q}) = \left\langle \sum_i \sum_j a_i a_j^{\star} \mathrm{e}^{\mathrm{i}\mathbf{q}\cdot\mathbf{r}_{ij}} \right\rangle, \tag{C.1}$$

where the sums run over all ions in the sample, $\mathbf{r}_{ij}$ is the distance between ions i and j and a_i is the scattering amplitude of the species to which i belongs (for example, the neutron scattering length in the case of neutron scattering). Because of the periodic boundary conditions, the accessible vectors **q** with a cubic simulation cell of side L are restricted to the set $\frac{2\pi}{L}(m, n, p)$ where m, n, and p are integers, and this provides a limit to the resolution of the simulated pattern.

We used the atomic position files obtained from the MD simulations on d-fluorite structures to calculate the diffuse scattering from equation (C.1). The MD patterns were obtained from simulations on 11 000 atoms. These simulations were between 31 and 100 ps long. We started them at 2000 K and the temperature was then lowered down to 300 K with a cooling rate lower than 50 K ps^{-1}. The Y^{3+} and Nb^{5+} atoms were placed at random on the cation lattice. We calculated $I(\mathbf{q})$ for the six equivalent ⟨110⟩ planes and averaged in order to show the data in the figure. We input the values of $I(\mathbf{q})$ on the grid of allowed **q** vectors into a contour program to generate the images shown in figure 8.

References

[1] Hull S 2004 *Rep. Prog. Phys.* **67** 1233–314
[2] Etsell T H and Flengas S N 1970 *Chem. Rev.* **70** 339–76
[3] Bogicevic A and Wolverton C 2003 *Phys. Rev.* B **67** 024106
[4] Zacate M O, Minervini L, Bradfield D J, Grimes R W and Sickafus K E 1999 *Solid State Ion.* **128** 243–54
[5] Kilo M, Argirusis C, Borchardt G and Jackson R A 2003 *Phys. Chem. Chem. Phys.* **5** 2219–24
[6] Krishnamurthy R, Yoon Y-G, Srolovitz D J and Car R 2004 *J. Am. Ceram. Soc.* **87** 1821–30
[7] Devanathan R, Weber W J, Singhal S C and Gale J D 2006 *Solid State Ion.* **177** 1251–8
[8] Norberg S T, Ahmed I, Hull S, Marrocchelli D and Madden P A 2009 *J. Phys.: Condens. Matter* **21** 215401
[9] Shannon R D 1976 *Acta Crystallogr.* A **32** 751–67
[10] Lee J H and Yoshimura M 1999 *Solid State Ion.* **124** 185–91
[11] Marrocchelli D, Madden P A, Norberg S T and Hull S 2009 *Solid-State Ionics—2008* (*Mater. Res. Soc. Symp. Proc.* vol 1126) ed E Traversa, T Armstrong, K Eguchi and M R Palacin (Warrendale, PA: Minerals, Metals and Materials Society) pp 71–8
[12] McGreevy R L 2001 *J. Phys.: Condens. Matter* **13** R877–913
[13] Tucker M G, Keen D A, Dove M T, Goodwin A L and Hui Q 2007 *J. Phys.: Condens. Matter* **19** 335218
[14] Norberg S T, Tucker M G and Hull S 2009 *J. Appl. Crystallogr.* **42** 179–84
[15] Miida R, Sato F, Tanaka M, Naito H and Arashi H 1997 *J. Appl. Crystallogr.* **30** 272–9
[16] Garcia-Martin S, Alario-Franco M A, Fagg D P, Feighery A J and Irvine J T S 2000 *Chem. Mater.* **12** 1729–37
[17] Whittle K R, Cranswick L M D, Redfern S A T, Swainson I P and Lumpkin G R 2009 *J. Solid State Chem.* **182** 442–50
[18] Jiang C, Stanek C R, Sickafus K E and Uberuaga B P 2009 *Phys. Rev.* B **79** 104203
[19] Hansen J-P and McDonald I R 1986 *Theory of Simple Liquids* (New York: Academic)
[20] Marrocchelli D, Salannne M, Madden P A, Simon C and Turq P 2009 *Mol. Phys.* **107** 443–52
[21] Subbarao E C and Ramakrishnan T V 1979 *Fast Ion Transport in Solids* ed P Vashista *et al* (New York: Elsevier/North-Holland) pp 653–6
[22] Kawata K, Maekawa H, Nemoto T and Yamamura T 2006 *Solid State Ion.* **177** 1687–90
[23] Goff J P, Hayes W, Hull S, Hutchings M T and Clausen K N 1999 *Phys. Rev.* B **59** 14202–18
[24] Zunger A, Wei S H, Ferreira L G and Bernard J E 1990 *Phys. Rev. Lett.* **65** 353–6
[25] Madden P A, Heaton R J, Aguado A and Jahn S 2006 *J. Mol. Struct.: THEOCHEM* **771** 9–18
[26] Tuckerman M E and Martyna G J 2000 *J. Phys. Chem.* B **104** 159–78
[27] Castiglione M J and Madden P A 1999 *J. Phys.: Condens. Matter* **13** 9963–83
[28] Castiglione M J, Wilson M and Madden P A 2001 *J. Phys.: Condens. Matter* **13** 9963–83